Climatic fingerprint of spring discharge depletion in the southern Italian Apennines from 1601 to 2020 CE

Nazzareno Diodato, Fredrik Charpentier Ljungqvist, Francesco Fiorillo, Libera Esposito, Gerardo Ventafridda, Gianni Bellocchi

▶ **To cite this version:**

PAPER • OPEN ACCESS

Climatic fingerprint of spring discharge depletion in the southern Italian Apennines from 1601 to 2020 CE

To cite this article: Nazzareno Diodato *et al* 2022 *Environ. Res. Commun.* **4** 125011

View the article online for updates and enhancements.

Environmental Research Communications

PAPER

Climatic fingerprint of spring discharge depletion in the southern Italian Apennines from 1601 to 2020 CE

Nazzareno Diodato[1], Fredrik Charpentier Ljungqvist[2,3,4,*] , Francesco Fiorillo[5], Libera Esposito[5], Gerardo Ventafridda[6] and Gianni Bellocchi[1,7]

1. Met European Research Observatory—International Affiliates Program of the University Corporation for Atmospheric Research, 82100 Benevento, Italy
2. Department of History, Stockholm University, 106 91, Stockholm, Sweden
3. Bolin Centre for Climate Research, Stockholm University, 106 91, Stockholm, Sweden
4. Swedish Collegium for Advanced Study, Linneanum, 752 38 Uppsala, Sweden
5. Department of Science and Technologies, University of Sannio, 82100 Benevento, Italy
6. Acquedotto Pugliese S.p.A, 70121 Bari, Italy
7. Université Clermont Auvergne, INRAE, VetAgro Sup, UREP, 63000 Clermont-Ferrand, France
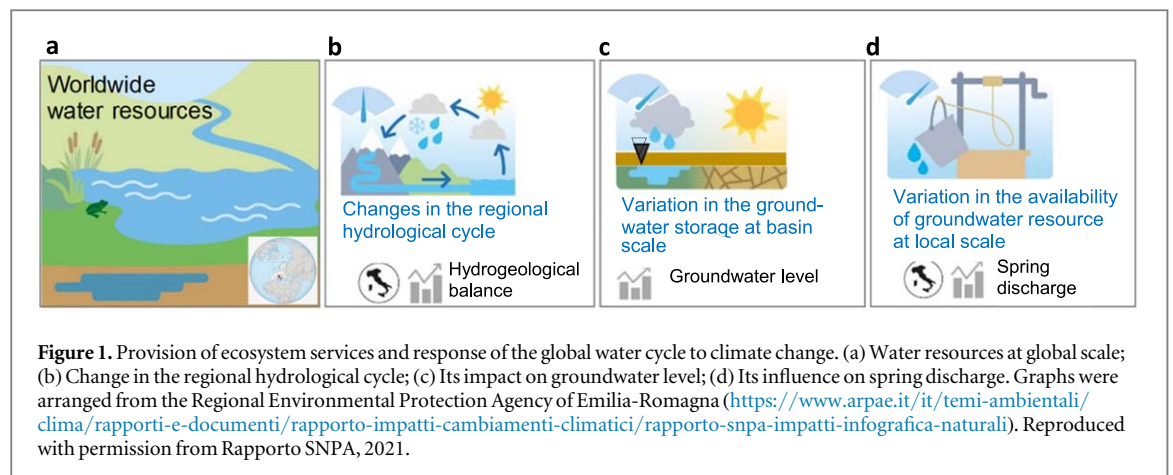* Author to whom any correspondence should be addressed.

E-mail: fredrik.c.l@historia.su.se

Abstract

Annual mean spring discharge (ASD) is an important water supply source, essential for ecological systems and societies dependent on groundwater resources. Influenced by both regional and local climate fluctuations, the inter-annual variability of ASD represents a climate memory signal, significantly affected when the drought pattern manifests itself in changing climatic regimes. Gaining a better historical perspective on ASD changes requires extended time-series of discharge data and relevant climate drivers. Here, using a parsimonious model, we present a continuous (modelled) time-series of annual ASD for the karst spring of Caposele, in the Cervialto Massif of southern Italy, which is hitherto the longest (1601–2020 CE) such time-series for the entire Mediterranean region. The model was designed to capture the importance of large-scale seasonal (spring, autumn and winter) precipitation (hydro-meteorological factor), and flood and drought indices (climatological factor), and to be consistent with a sample (1920–2020 CE) of actual data. We show a limited overall sensitivity of ASD to climate variability, with a mean of 4.21 $\mathrm{m}^3\,\mathrm{s}^{-1}$ and a drop from ∼1759 CE. With a mean value of ∼3.60 $\mathrm{m}^3\,\mathrm{s}^{-1}$ after ∼1987 CE, ASD has revealed a substantial descending trend—possibly a fingerprint of recent warming—with a depletion of regional water reservoirs. These results highlight the need to strengthen the capacity of groundwater resources in the face of changing, and possibly enhanced, drought patterns in the Mediterranean region.

1. Introduction

The Earth's climate has changed in historical times (Pfister and Wanner 2021) and is expected to continue to change in a warming world, in ways that vary from region to region and are not always predictable (due to confounded uncertainties, e.g. Anchukaitis and Smerdon 2022), with implications for water resources, ecosystems and human societies (Braconnot and Vimeux 2020). Spring discharges, in particular, are important for the supply of drinking water (Ranjan and Pankaj 2021) and for the development and maintenance of reservoir-based hydropower (Dorber *et al* 2020) in much of the Northern Hemisphere. They also provide nutrients to rivers and support marine productivity (Liang and Zhang 2021). Climate variations induce considerable inter-annual fluctuations in spring discharge, especially in mountainous areas, where groundwater is irregularly recharged by rainfall and snowmelt (Rao *et al* 2020). Understanding climate-related changes in

Figure 1. Provision of ecosystem services and response of the global water cycle to climate change. (a) Water resources at global scale; (b) Change in the regional hydrological cycle; (c) Its impact on groundwater level; (d) Its influence on spring discharge. Graphs were arranged from the Regional Environmental Protection Agency of Emilia-Romagna (https://www.arpae.it/it/temi-ambientali/clima/rapporti-e-documenti/rapporto-impatti-cambiamenti-climatici/rapporto-snpa-impatti-infografica-naturali). Reproduced with permission from Rapporto SNPA, 2021.

groundwater recharge and discharge is particularly important for understanding the spatial and temporal responses of stream ecosystems to land development (Hare *et al* 2021).

Climatic droughts (i.e. precipitation deficiencies compared to annual or seasonal averages) and their hydrological, agronomic and ecological consequences often result in random shortages of water resources where water is demanded (Kogan *et al* 2020). In the Mediterranean region, in particular, the consequences of precipitation deficits can be severe, due to the relative scarcity of water resources, high demand due to human activities, and soil degradation processes in this area (Diodato and Bellocchi 2008). However, compared to studies on surface water, those on groundwater discharge remain limited (Li *et al* 2019). Some research indicates that altered climate regimes, both globally (Wang *et al* 2018, Cuthbert *et al* 2019, Pokhrel *et al* 2021) and regionally (Manna *et al* 2019, Tegel *et al* 2020, Jaafarzadeh *et al* 2021), can have marked effects on groundwater storage and thus on spring discharge flows and the continued provision of ecosystem services at the local scale (Ouyang *et al* 2020) (figure 1).

In this way, climatic variability and changing precipitation regimes with changes in land use and land cover can have important impacts on sub-surface hydrological processes (Chen *et al* 2017), water infiltration (Cao *et al* 2018), recharge (Jaafarzadeh *et al* 2021) and thus water discharge (Fiorillo 2009, Manna *et al* 2019). In order to indicate what influence the position (flat or inclined) and nature of the soil layers (e.g. cracking and rock strata) have on the absorption of rainwater and what relationship they have with sources and water discharge in mountain caves, the Italian Renaissance polymath Leonardo da Vinci (1452–1519 CE) wrote on sheet 3r of the *Leicester code* that in his time (De Lorenzo 1939, p. 246, our translation):

> […] in the mountains, where the slopes in the rocks are placed oblique or by right, being interposed of little Earth, rainwater immediately penetrates into it, and flowing through the cracks absorbs the water, and fills the cracks and strata within the rock.

Subsequently, the scientific revolution of Nicolaus Copernicus (1473–1543), Galileo Galilei (1564–1642) and Isaac Newton (1642–1727) led to the formulation of the laws governing the physics of motion, and the subsequent physical-mathematical developments of the 18th and 19th centuries gave rise to the dream of being able to predict the evolution of any physical system if one knows the acting forces well enough. In 1814, the French mathematician Pierre-Simon Laplace (1749–1827) stated (Fuccello 2021, p. 16, our translation):

> We must consider the present state of the […] as the effect of a given previous state and as the cause of what will be in the future. An intelligence that, in a given instant, knew all the forces that animate nature […] for such intelligence everything would be clear and certain and so would the future as well as the past be present.

The same principle applies to spring water flows, but today, although the accurate measurement of proxy factors that control the infiltration processes involved in the evolution of recharge (Philipps *et al* 2004, Gates *et al* 2008, Li *et al* 2019, Mankin *et al* 2019), only a few simple models have been developed for the long-term historical description of annual spring discharge (Lamoureux *et al* 2006, Dubois *et al* 2020, Nolin *et al* 2021). Thus, the historical reconstruction of groundwater discharge and its prediction still remains a challenge for environmental engineering and hydrogeology (Diodato *et al* 2017, Zhang *et al* 2020, Xu *et al* 2021). In addition, projections from different general circulation models that make a global assessment of the effects of climate

change on hydrological regimes are highly divergent (Sperna Weiland *et al* 2011). There is also a need to further verify the most recent results based on Earth System Models (Cui *et al* 2020).

Recent climate changes in southern Italy have been manifested by changes in the temporal and spatial patterns of precipitation (Caloiero *et al* 2018, Ljungqvist *et al* 2019), as well as in several other regions of the world (Ljungqvist *et al* 2016). In particular, Ducci and Tranfaglia (2008) assessed water balance variations caused by precipitation and temperature changes in the Campania region (13590 km^2 around 40° N and 14 °E). More recently, Leone *et al* (2021) inferred the relationship between spring discharge and climatic variables in Caposele during a 100-year period (1920–2020).
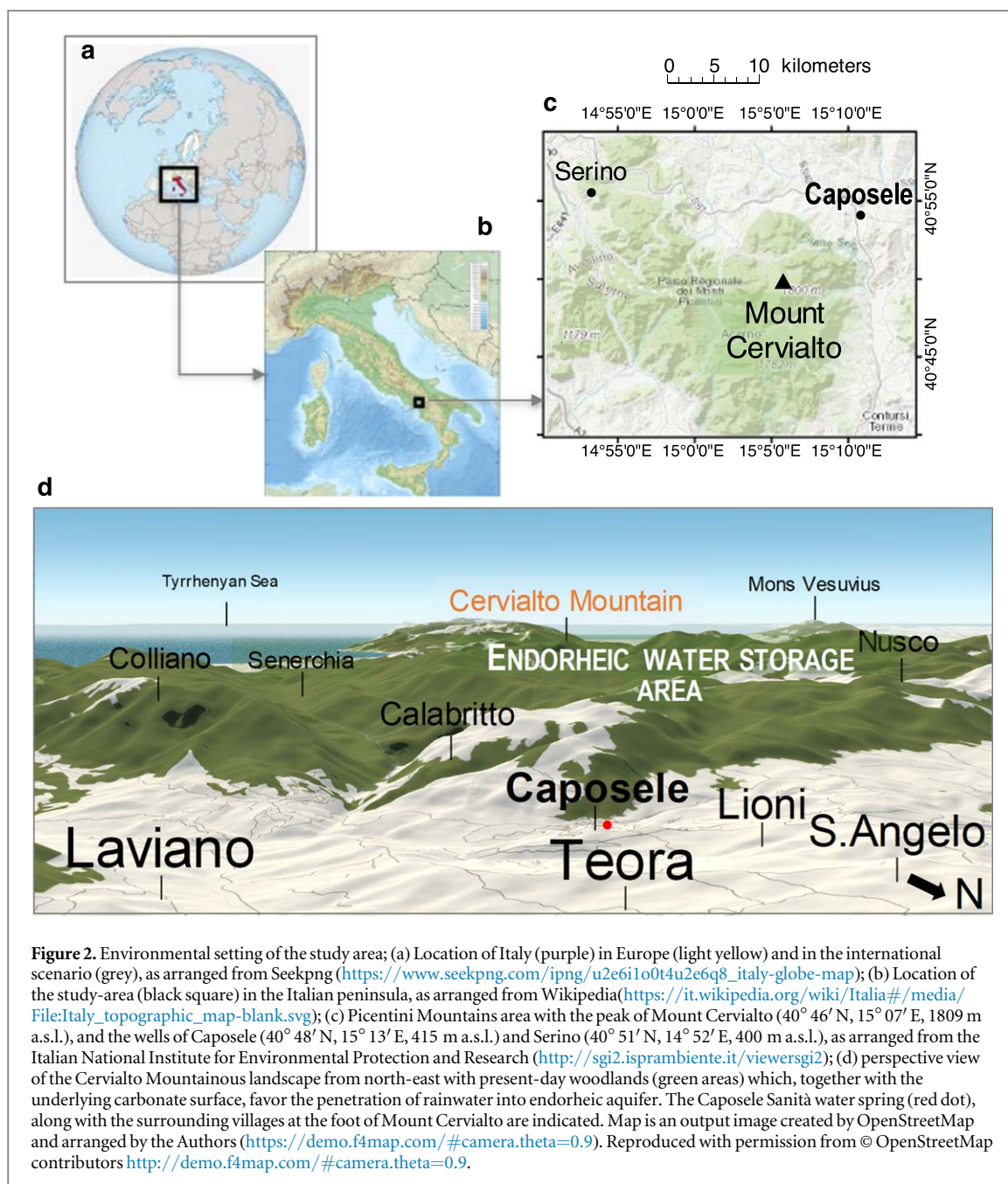
A proper understanding of the response of discharge to the water cycle and human activities can improve water resource management. In particular, through water cycle exchanges, groundwater discharge zones generate an active hydrogeological connection. These hydrological components can be simulated using lumped or distributed models (Hsu *et al* 2012). Although a hydrological system can be modelled using an integrated, distributed approach to surface groundwater discharge, downscaling of precipitation is a source of uncertainty and can produce misleading results in groundwater response. On the relationship between the standard precipitation index and the karstic spring, Fiorillo (2009) and Fiorillo and Guadagno (2010) concluded that a prolonged lack of cumulative rainfall causes a reduction in spring discharge during the following year. This indicates a memory effect of the karstic aquifer and a more complex relationship between rainfall and discharge. Inter-annual and multi-decadal variations in precipitation in the Mediterranean are often the result of variations in the North Atlantic Oscillation (NAO), a meteorological phenomenon over the North Atlantic Ocean that consists of fluctuations in the difference in atmospheric pressure at sea level between the Icelandic Low and the Azores High (Ait Brahim *et al* 2018). NAO can have a substantial influence on groundwater resources in terms of changes in the quantity, duration and location of groundwater recharge, discharge and fluctuation (De Vita *et al* 2012, Fiorillo *et al* 2015). However, historical variations and interactions between climate, groundwater and ecosystem services are still poorly understood (Qiu *et al* 2019, Saccò *et al* 2021), partly due to the difficulty of modelling and reconstructing water discharge/recharge over longer periods. Owing to these unexplored patterns and the lack of cross-references between environment, discharge, climate and history, it can be difficult to make connections between these disciplines.

In order to promote interdisciplinary research on spring discharge dynamics, this article aims to bridge the gap between the vast amount of knowledge reported in water research and the limited availability of data for historical modelling. It describes the concepts and methods used in a parsimonious model, the Historical DIScharge CLIMatological Model (HDISCLIM), which was developed to reconstruct the longest annual time-series of spring discharge (ASD) in the Mediterranean region. The proposed model—HDISCLIM—is parsimonious, based on simplified inputs such as seasonal precipitation, and drought and floods indicators, to overcome the limitations imposed by more sophisticated, physically-based models. Once calibrated and validated, the model was applied to estimate ASD long before the monitoring period, across different climatic periods, including the latter part of the Little Ice Age (here, 1601–1850 CE) and the most recent warm period (here, 1851–2020 CE).

2. Study-area, data and methods

2.1. Study-area

The Caposele aquifer (our study-site) is located in southern Italy, along the Apennine chain, where there is the highest potential for active groundwater recharge in the entire Italian peninsula (figures 2(a), (b)). The aquifer is located within the Cervialto Massif basin (figure 2(d)), which has not been affected by changes in land use or other anthropogenic activities over time, making the Caposele station unique for studying the effect of climate patterns on groundwater discharge (Leone *et al* 2021). In particular, groundwater recharge in central-southern peninsular Italy has been supported by high annual precipitation, especially along the west (Tyrrhenian) side (figure 3(a)). Wide endorheic zones characterise these mountains and play an important role in the recharge processes (figure 2(d)). The origin of these endorheic zones is related to upper Pliocene–Pleistocene tectonic activity, which caused a general uplift by normal faults and formation of graben zones (Fiorillo *et al* 2015). During the subsequent continental environment (Pleistocene-Holocene), karst processes have transformed these zones in endorheic ones, allowing the complete absorption of runoff. The largest endorheic area is the Laceno Plain (20.5 km^2), where there is a small sinking lakes that increases during the winter–spring period. The aquifer is developed within the northern sector of the Picentini chain (Mount Cervialto, figure 2(c)), a limestone and limestone-dolomitic massif, tectonically overlain by terrigenous and impermeable deposits, constituting clay complexes. The massif constitutes a large karstic aquifer and feeds the Sanità spring, located within the village of Caposele (figure 2(c)), with a mean annual discharge of $\sim$4 m^3 s^{-1} (Fiorillo 2009, Fiorillo and Doglioni 2010).

Figure 2. Environmental setting of the study area; (a) Location of Italy (purple) in Europe (light yellow) and in the international scenario (grey), as arranged from Seekpng (https://www.seekpng.com/ipng/u2e6i1o0t4u2e6q8_italy-globe-map); (b) Location of the study-area (black square) in the Italian peninsula, as arranged from Wikipedia(https://it.wikipedia.org/wiki/Italia#/media/File:Italy_topographic_map-blank.svg); (c) Picentini Mountains area with the peak of Mount Cervialto (40° 46′ N, 15° 07′ E, 1809 m a.s.l.), and the wells of Caposele (40° 48′ N, 15° 13′ E, 415 m a.s.l.) and Serino (40° 51′ N, 14° 52′ E, 400 m a.s.l.), as arranged from the Italian National Institute for Environmental Protection and Research (http://sgi2.isprambiente.it/viewersgi2); (d) perspective view of the Cervialto Mountainous landscape from north-east with present-day woodlands (green areas) which, together with the underlying carbonate surface, favor the penetration of rainwater into endorheic aquifer. The Caposele Sanità water spring (red dot), along with the surrounding villages at the foot of Mount Cervialto are indicated. Map is an output image created by OpenStreetMap and arranged by the Authors (https://demo.f4map.com/#camera.theta=0.9). Reproduced with permission from © OpenStreetMap contributors http://demo.f4map.com/#camera.theta=0.9.

The spring feeds a main water distribution system, the Apulian Aqueduct (*Acquedotto Pugliese*), which supplies water to a large area of the Apulia region (19,345 km^2 around 41 °N and 16 °E), adjacent to Campania in south-eastern Italy. Locally, there is a Mediterranean climate, characterised by dry, warm summers and wet periods occurring in autumn, winter and spring. The mean annual precipitation and temperature of the spring catchment are 2109 mm and 8.5 °C, respectively (Fiorillo *et al* 2015); snowfall generally occurs during winter above 1000 m a.s.l.

Mount Cervialto is covered by dense tree vegetation (figure 2(d)), where the isolation created by the foliage leads to almost constant climatic conditions in the undergrowth, which plays an important role in evapotranspiration and for the hydrogeological budget of the area (Civita and Rostagno 2014). Based on the worlwide application of the Thornthwaite method (Willmott *et al* 1985), the amount of evapotranspiration was calculated for the Cervialto area where, when climatic conditions permit it, the amount of rain is free to percolate and recharge the karst aquifer (figure 3(b)). Based on the monthly precipitation and evapotranspiration patterns (figure 3(c)), autumn is the wettest season, but snowmelt in winter and spring can provide a considerable amount of water to keep the aquifer replenished. In this way, the extensive and widespread endorheic mountain areas favour recharge processes during all rainy seasons of the karst massif, although the effective precipitation is close to zero in summer due to the high evapotranspiration rate (water deficit) during this season (figure 3(c),

Figure 3. Rainfall pattern and groundwater discharge zones establishing active hydrologic connectivity through water cycle exchange (large arrows). (a) Mean annual precipitation (1971–2000 CE) over southern peninsular Italy, with the identification of Cervialto Mountains area (white squared) (arranged by ordinary cokriging via ArcGIS Geostatistical Analyst (Environmental Systems Research Institute) on SCIA (*Sistema nazionale per la raccolta, elaborazione e diffusione di dati climatologici di interesse ambientale*) data http:// www.scia.isprambiente.it/wwwrootscia/Home_new.html); (b) Climatic variables involved in the water cycle that drive groundwater discharge in a typical mountainous karst aquifer (arranged from CrushPixel https://www.crushpixel.com/it/stock-vector/Sun- with-clouds-illustration-vector-2952907.html, the United States Geological Survey https://www.usgs.gov/special-topics/water- science-school/science/aquifers-and-groundwater?qt-science_center_objects=0#qt-science_center_objects and the Geological Survey https://www.gsi.i.e./en-i.e./programmes-and-projects/groundwater/activities/understanding-irish-karst/karst- landforms/Pages/default.aspx); (c) Thornthwaite modified hydrological water balance over the Cervialto area for the period 1981–2010 arranged from an updated version of the WebWIMP programme - WebWIMP 1.01 - as implemented at the University of Delaware (USA) in 2003 via http://climate.geog.udel.edu/~wimp/index.html (Willmott *et al* 1985). Reproduced with permission from CrushPixel http://www.crushpixel.com/it/stock-vector/sun-with-clouds-illustration-vector-2952907.html © 2022. Repro- duced from Geological Survey Ireland. Geological Survey Ireland is a Division of Department of the Environment, Climate and Communications © 2022.

beige band). As autumn progresses, rainfall increases and evapotranspiration decreases, with active groundwater recharge (GWR) starting in November and available until May (figure 3(c), blue bands).

2.2. Data analysis

The HDISCLIM was developed on spring discharge data provided by Diodato and Fiorillo (2013), updated to 2020, and seasonal precipitation data derived from Pauling *et al* (2006), updated to 2020 by the GPCC V5 analysis, as provided via Climate Explorer (Trouet and Van Oldenborgh 2013) for the grid-point including the Mount Cervialto aquifer (spatial resolution of 0.25°, i.e. ∼25 km × 25 km). Flood and drought indices, *FI* and *DI*, were provided by Diodato *et al* (2019), and Diodato and Bellocchi (2011), respectively. To represent drought control, we used the time-series of *DI* values from central-southern Italy Diodato and Bellocchi (2011), while to capture flood control on groundwater discharge, we based the extraction of local *FI* inputs on the written sources used by Diodato *et al* (2019) to provide baseline index values for Italy, which are for the southern Calore River Basin (Diodato *et al* 2017) in the Picentini-Cervialto Mountains. This implies that different scaling factors were applied to downscale these areal estimates to the Caposele study site, i.e. β (for *FI*) and square root (for *DI*) in equation (3).

For the purpose of modelling, the period of available data was split into a calibration period (1949–2020 CE) and a validation period (1920–1948 CE), i.e. roughly 2/3 and 1/3 of the actual dataset. Spreadsheet-based model building was carried out with the help of the online statistics programme STATGRAPHIC (http://www. statpoint.net/default.aspx), with graphical assistance provided by WESSA (https://www.wessa.net/tsa.wasp) and CurveExpert Professional 1.6 (https://www.curveexpert.net).

The modelling procedure was carried out by iteratively calibrating model the parameters A of equation (2) and α, β and φ of equation (3) in order to match the following criteria:

$$\begin{cases} R^2 = \max \\ |b - 1| = 0 \\ MAE = \min \end{cases} \tag{1}$$

where R^2 (optimum 1) is the goodness-of-fit of the linear regression of observations versus estimates ($r = \sqrt{R^2}$ being the correlation coefficient quantifying the strength of the linear relationship between the two variables), $|b - 1|$ is the difference from the unity of the regression slope (b, optimum 1) between actual and modelled data, MAE (optimum 0) is the mean absolute error. Our model does not incorporate uncertainty directly and the uncertainty of its output was evaluated separately. First, we provide the standard errors of parameters (intercept and slope) of the regression of the observations against the estimates for the calibration stage. Then, the Nash–Sutcliffe efficiency index ($-\infty < EF \leqslant 1$, optimal; Nash and Sutcliffe 1970) was calculated as an indicator of model performance uncertainty, as values above 0.6 indicate limited model uncertainty, likely associated with narrow parameter uncertainty (Lim *et al* 2006). The Kolmogorov-Smirnov test (Smirnov 1948) was used to verify that the observed and estimated data samples had the same statistical distribution and a post-reconstruction Gaussian filter was applied (AnClim, (http://www.climahom.eu/AnClim.html; Stepanek 2007) to reduce uncertainties due to the existence of noise in the estimated results.

Two types of homogeneity test (i.e. Mann-Whitney-Pettit test and the SNHT) were also performed with AnClim to identify possible shifts in the mean value of the spring discharge time-series (i.e. change-point years or break-point years). The SNHT (Standard Normal Homogeneity Test) compares the mean of the data on the previous period observations and the following period observations, and normalises by the standard deviation. The Mann-Whitney-Pettit test works in a similar way, but it is a non-parametric rank test. The comparison of detected change-point years is recommended because the SNHT more easily detects breaks at the beginning and end of the time-series (or both in its double-shift variant), while the Mann-Whitney-Pettit test is more sensitive to breaks in the middle of the time-series (Toreti *et al* 2011).

Gumbel plots, a standard graphing tool used in extreme value theory that helps judge the fit of the distribution, were performed based on generalised extreme value (gev) distributions (Coles 2001), as provided by Climate Explorer (Trouet and Van Oldenborgh 2013).

We computed the Hurst (1951) exponent H (chaos rate), which is connected to the time-series' fractal dimension D = 2-H, to determine the long-term dependency and appraise the cyclical patterns. Long memory arises when $0.5 < H < 1.0$, i.e. very distant events are associated because correlations fade slowly. Short-distance dependence ($0.0 < H < 0.5$), on the other hand, is characterised by rapidly fading correlations. Using the memory analysis software SelQoS (Self-similarity and QoS analysis tool (Ramírez-Pacheco *et al* 2008), we referred to two approaches, both of which are credited with being fairly effective at predicting H (Belov *et al* 2006): the commonly used rescaled range analysis, or R/S method, and the residual variance ratio method, which is known to be unbiased. A criterion of H = 0.65 is utilised to select a time-series that can be successfully predicted.

The wavelet power spectrum with Morlet basis function was presented as a time–frequency graph to identify potential nonstationary oscillations at different frequencies in the time-series, using the Paleontological Statistics Software Package for Education and Data Analysis (PAST) by Hammer *et al* (2001).

2.3. Methods: modelling of the annual spring discharge

We derived a modelling approach balancing simplicity and complexity, with the ability to both explain hydrological and climatological properties and to predict the inter-annual dynamics of spring discharge (Dawid and Senn 2011). The Historical DIScharge CLIMatological Model (HDISCLIM) linearizes, $A \cdot (X + Y)$, and simplifies to four parameters the seminal, five-parameter power-based function $A \cdot f(X)^B$ described by Diodato and Fiorillo (2013). Linearization was achieved by setting the shape parameter B equal to 1, which facilitates convergence of parameter estimation. Then, components were represented in the model that are considered significant for the problem to be solved, taking into account relevant aspects of the real system and of the modeller's perception. Specifically, to predict the annual spring discharge, two independent components (*X* and *Y*) represent the hydro-meteorological (*HMF*) and climatological (*ClimF*) factors, respectively, expressed by the following relationship:

$$HDISCLIM_{(y=0)} = A \cdot (HMF + ClimF) \tag{2}$$

where $HDISCLIM_{(y=0)}$ is the spring discharge ($m^3 s^{-1}$) at Caposele-Sanità station for the current year ($y = 0$), with the scale parameter A converting the value in brackets to $m^3 s^{-1}$. Substituting the relative terms in brackets, we obtained the following equations:

$$HMF = (\alpha \cdot \sqrt{P_{Aut(y-1)} + P_{Win(y)}} + P_{Spr(y)}) \cdot (\beta \cdot FI + \sqrt{\varphi - DI}) \qquad (3)$$

where the P_{Aut}, P_{Win} and P_{Spr} (mm) are the precipitation amounts falling in autumn, winter and spring, respectively, as derived from large-scale precipitant systems; P_{Aut} and P_{Win}, however, have a different weight than spring precipitation, due to lower evapotranspiration and winter snowfall; y represents the current year, while y-1 identifies the antecedent year as memory effect; α and β are scale parameters. Esit *et al* (2021) concurred in this aspect and reported how multi-seasonal to multi-annual memory of deep soil moisture and groundwater can also contribute to hydroclimate predictability. In particular, the positive change of first term under root represents the soil water deficit during the transition from the arid to the wet season in autumn. For this purpose, the sum of the rainfall that the basin receives in these months is of primary importance. The infiltration capacity is maximum in this period of the year since the soil became dry in summer, and thus the soil was more conductive to the effects of soil properties on infiltration processes. The others two seasonal term of precipitation represent the water infiltrations in winter and spring, respectively, similar to relationships to the seasonal contrasts in the precipitation scaling closely mirrored by those in the moisture convergence change referred by Liang and Zhang (2021).

FI and DI are the flood and drought indices, respectively. These two climatological indices provide integrated information on the local rainfall abundance and aridity, respectively (Diodato and Bellocchi 2011, Diodato *et al* 2019). Following Nowreen *et al* (2020) and Cruz *et al* (2021), a drought index reflects changes in temperature and precipitation, while a flood index reflects a surplus of water availability for recharging. Thus, the combined use of these indices makes it possible to capture both persistent water deficits and the short-term climatological component of groundwater recharge. FI as a proxy variable of storm water infiltration was suggested in the relationship between groundwater flow and water intrusion by Costall *et al* (2020). FI is an important input variable, as even in years with low autumn to spring precipitation, large discharge/recharge cycles can be produced, as observed in dry and wet regions worldwide.[11] It was determined as a binary variable. In particular, the calibration work resulted in setting FI equal to 1 if one or more floods occurred in a year (with $FI = 0$ otherwise). The term DI represents the duration between storms and is a proxy of the extent of the annual drought. DI can assume different values depending on the number of continuous months of drought. As, in fact, Wu *et al* (2020) referred to, the storage capacity for groundwater is imposed by the stress on water resources and the increase in the probability of severe drought occurrence. The climate factor in equation (1) is expressed as:

$$ClimF = P_{Aut(y-2)} + P_{Spr(y-1)} + P_{Sum(y-1)} \qquad (4)$$

where P_{Sum} is the amount of precipitation in summer (mm), and y–2 identifies the previous two years. Taking into account the years preceding to discharge estimate is important because the water, from the time it is received as precipitation from the basin to the source, takes a time-lag that the model interprets with this delay and that can vary from one place to another.

The parameterisation of the model was derived from physical and statistical considerations that were integrated with the observed correlations, and included the issue of downscaling via a hydrological function, equation (2). In particular, the model assumptions were derived deductively from established physical principles, which nevertheless include a certain level of empirical generalisation (e.g. the climatic background of precipitation) to allow operating at an appropriate environmental scale, transforming inputs into reliable outputs, statistically consistent with observations. The mathematical formulation of the process under study was thus designed at a point-station via the spatial disaggregation of a homogeneous unit area. The spring discharge model was designed not to contain a position parameter, i.e. a constant term prescribing the fixed quantity that contributes to the spring discharge when all other terms of the equation are equal to zero. A fixed parameter could cause a biased response in the estimated long-term time-series, as the baseline groundwater discharge is likely to change as conditions change. In this way, the model predicts zero groundwater discharge for zero input values (Diodato *et al* 2021).

3. Results and discussions

3.1. Model evaluation

The ASD data resource of Caposele for the period 1949 to 2020 was used as the calibration dataset. The year 1981 was discarded due to the hydrological anomaly associated with the strong Earthquake of 23 November 1980 in Irpinia-Basilicata, which caused a significant increase in the flow of the Caposele spring (5.70 m s^{-1}), which returned to normal after more than a year (Esposito *et al* 2001). The calibration dataset (71 years) shows a rather wide variability of ASD values (from 2.95 m s^{-1} in 2002 to 5.11 m s^{-1} in 1960) and the performance of the model is satisfactory (according to a set of performance metrics and test statistics), which supports the robustness of the model to contrasting climatic conditions. In fact, although short in time, the calibration period covers two climatic regimes, characterised in Italy by a decrease in temperature and weak westerly winter winds until *c.* 1976, and strong increase in temperature and westerly winter winds thereafter (Diodato and Mariani 2007).
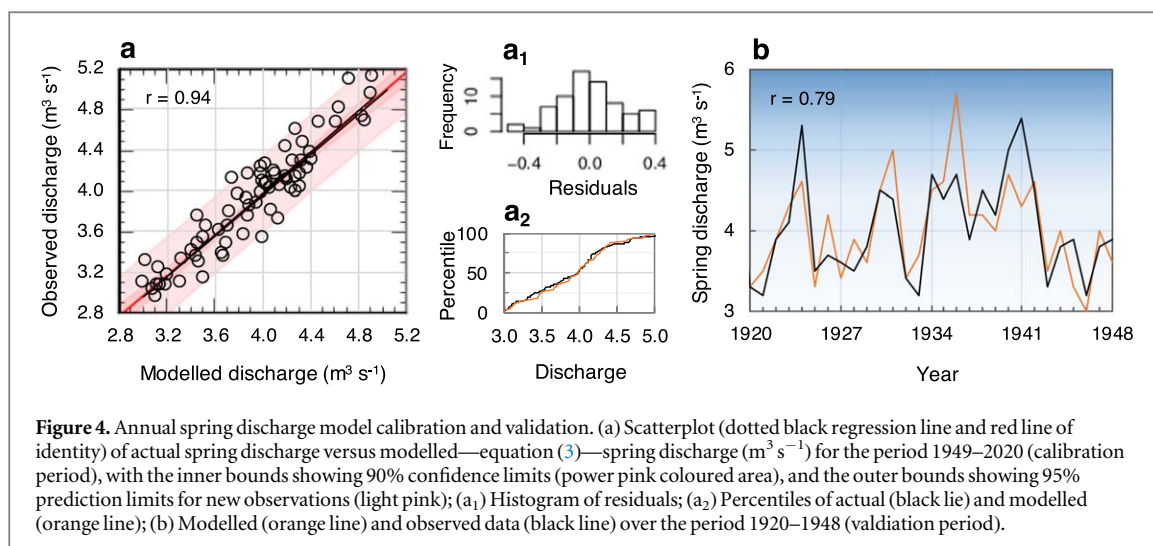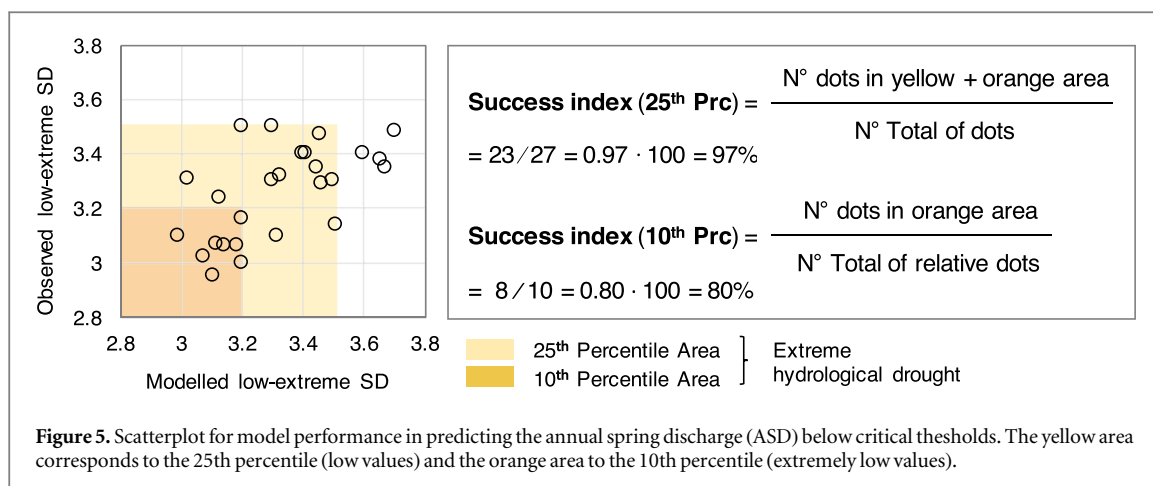
Figure 4. Annual spring discharge model calibration and validation. (a) Scatterplot (dotted black regression line and red line of identity) of actual spring discharge versus modelled—equation (3)—spring discharge (m³ s⁻¹) for the period 1949–2020 (calibration period), with the inner bounds showing 90% confidence limits (power pink coloured area), and the outer bounds showing 95% prediction limits for new observations (light pink); (a₁) Histogram of residuals; (a₂) Percentiles of actual (black lie) and modelled (orange line); (b) Modelled (orange line) and observed data (black line) over the period 1920–1948 (valdiation period).

A highly significant relationship (F-test p∼0.00) was obtained between observations and predictions with the following parameter values: $A = 0.00098036$ in equation (2), and $\alpha = 40$, $\beta = 0.40$ and $\varphi = 12$ in equation (3). The linear regression between actual and estimated data had intercept a $= -0.06$ (± 0.18 standard error) m³ s⁻¹ and slope b $= 1.01$ (± 0.05 standard error). We obtained a mean annual spring discharge estimate of 3.92 m³ s⁻¹ (± 0.49 m³ s⁻¹ standard deviation), which is close to the mean of the actual data of 3.90 m³ s⁻¹ (± 0.53 m³ s⁻¹ standard deviation). The calibrated model gave 2.99 m³ s⁻¹ in 1989 and 4.91 m³ s⁻¹ in 1960 as minimum and maximum estimates, respectively. There is no statistically significant difference between the two distributions (Kolmogorov-Smirnov p $= 0.09$), and the standardised skewness and kurtosis values between -2 to $+2$ (0.53 and -0.18, and -0.96 and -1.02 for actual and estimated values, respectively) indicate a non-significant departure from normality for both distributions.

Figure 4(a) reports the results of the calibration, where negligible departures of the data-points from the 1:1 identity line are observed (r $= 0.94$, equivalent to $R^2 = 0.88$). The Nash–Sutcliffe efficiency value (EF $= 0.88$) indicates limited uncertainty in the model estimates. The mean absolute error (MAE) was equal to 0.15 m³ s⁻¹, which is smaller than the standard error of the estimates (0.19 m³ s⁻¹). Figure 4(a₁) shows a Gaussian-like, skew-free distribution of the model residuals. The percentile distribution of the modelled spring discharge (figure 4 (a₂), orange line) approached the distributional shape of the observed discharge (figure 4(a₂), black line), indicating a satisfactory prediction over the range of ASD values (including low and high data). Since the Durbin-Watson (DW) statistic (DW $= 1.87$) has a p-value greater than 0.05 (p $= 0.27$), there is no indication of serial autocorrelation in the residuals.

Figure 4(b) shows the validation results for the homogenised time-series of 29 data-points, where the estimated (orange line) and the observed (black line) are reported. Although we see that some points deviate from the actual data (e.g in 1936), the correlation coefficient (r) was 0.79, with MAE $= 0.53$ m³ s⁻¹ (lower than the standard error of the estimates, equal to 0.69 m³ s⁻¹). Also in this case, there is no significant autocorrelation in the residuals (DW $= 2.12$; p $= 0.67$), both distributions are similar (Kolmogorov-Smirnov p $= 0.82$) and quasi-normal (standardised skewness and kurtosis values of 0.86 and 1.48, and -1.16 and 0.30 for actual and estimated values, respectively). The 1936 overestimate (4.7 against 3.7 m³ s⁻¹) is likely associated with the regionally aggregated autumn (1935) and winter (1936) precipitation data used as model inputs (276 and 267 mm, respectively), which appear to greatly exceed the locally measured data near Caposele (154 and 151 mm, respectively; SIMN, 1921–1997, available thorugh https://www.isprambiente.gov.it/it/progetti/cartella-progetti-in-corso/acque-interne-e-marino-costiere-1/progetti-conclusi/progetto-annali). This is the type of uncertainty that is expected when making long-term retrospective estimates, for which the adequacy of the model may be reflected less in the estimation of individual data points than in capturing intra- and inter-decadal patterns.

As the reconstruction of low to extremely low ASD values is critical, as they represent the most adverse situations for society and the environment, the predictive part of the model for these values requires thorough investigation. To this end, we developed a scatterplot (figure 5) showing all years in which, over the entire observation dataset (both calibration and validation data), the values were below the 25th percentile (yellow area + orange area) of the graph and the only years in which they were below the 10th percentile (orange area). When the points fall in the same area, it means that both values (observed and predicted) are below the 25th and 10th percentile, otherwise the model is in error. In this case, it appears that, for the 25th percentile threshold, the model gives a total success rate of 97%, while for the 10th percentile it gives a result of 80%.

Figure 5. Scatterplot for model performance in predicting the annual spring discharge (ASD) below critical thesholds. The yellow area corresponds to the 25th percentile (low values) and the orange area to the 10th percentile (extremely low values).

From these results, it can be deduced that the model satisfactorily reconstructs both types of hydrological drought (with low and extremely low ASD values).
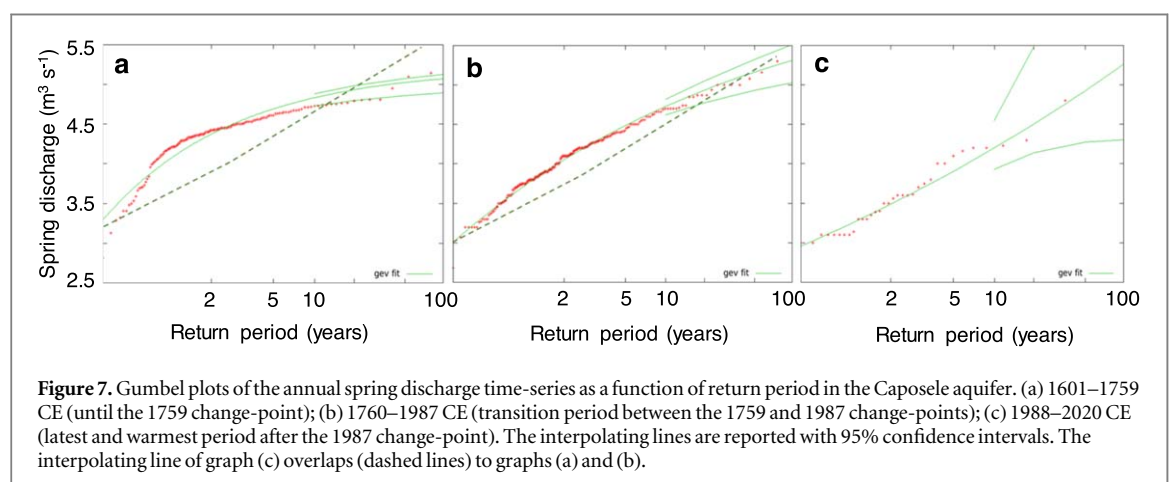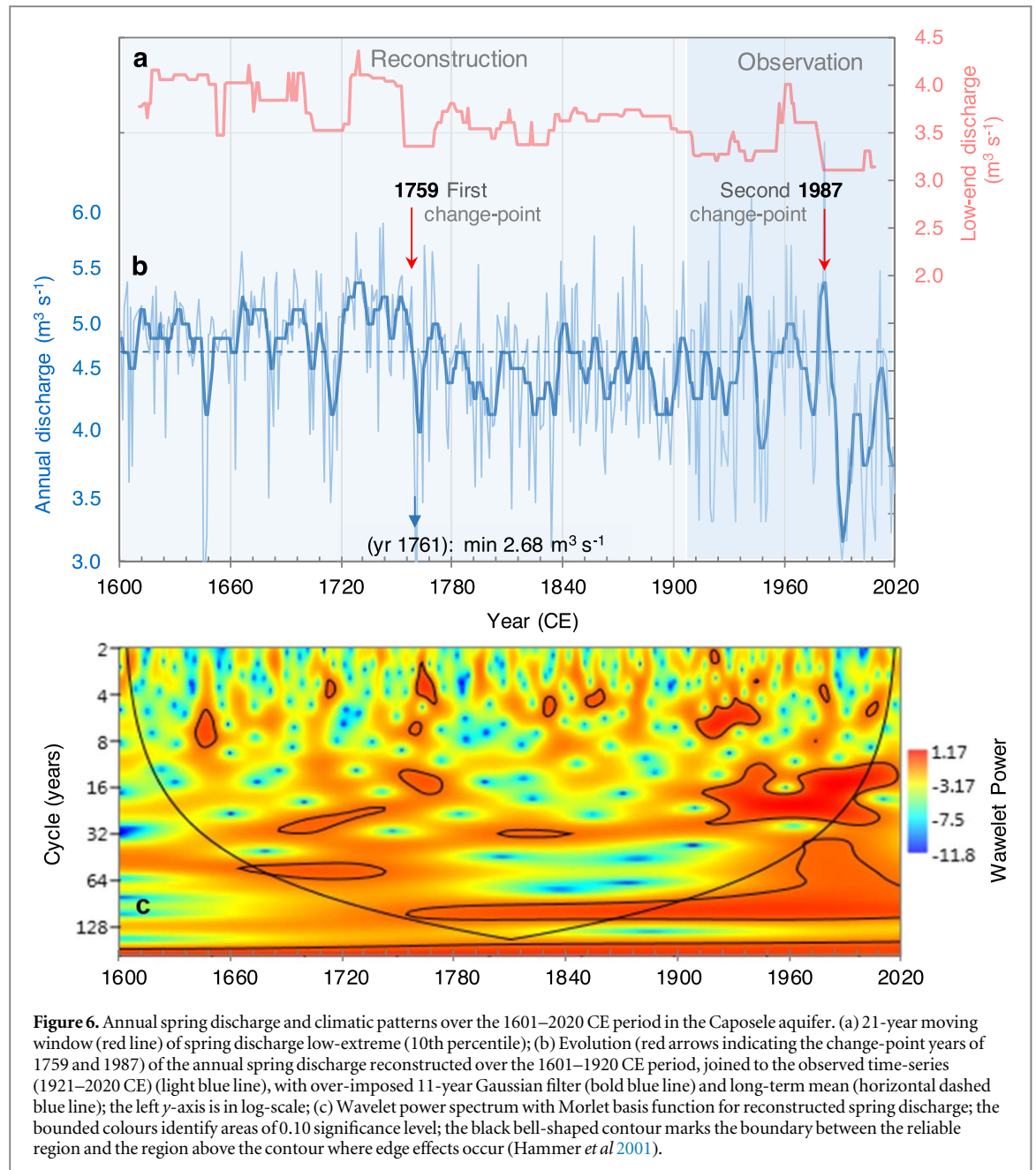
3.2. Historical evolution of spring discharge

In addition to highlighting the variability of spring discharge during the observation period (1920–2020 CE) at Caposele, our long-term reconstruction provides insights into the range of variability of the reconstruction during the years 1601–2020 CE, covering the final stages of the Little Ice Age (LIA; ~1300–1850 CE), a period marked by generally cold temperatures (Matthews and Briffa 2005, Ljungqvist *et al* 2012, Miller *et al* 2012, Wanner *et al* 2022), and the transition to the modern warming period (1851–2020 CE). Figure 6(b) shows the evolution of ASD time-series (blue line) and its 11-year Gaussian filter (bold blue line), with a relatively constant inter-annual variability over a long period, except for the most recent times.
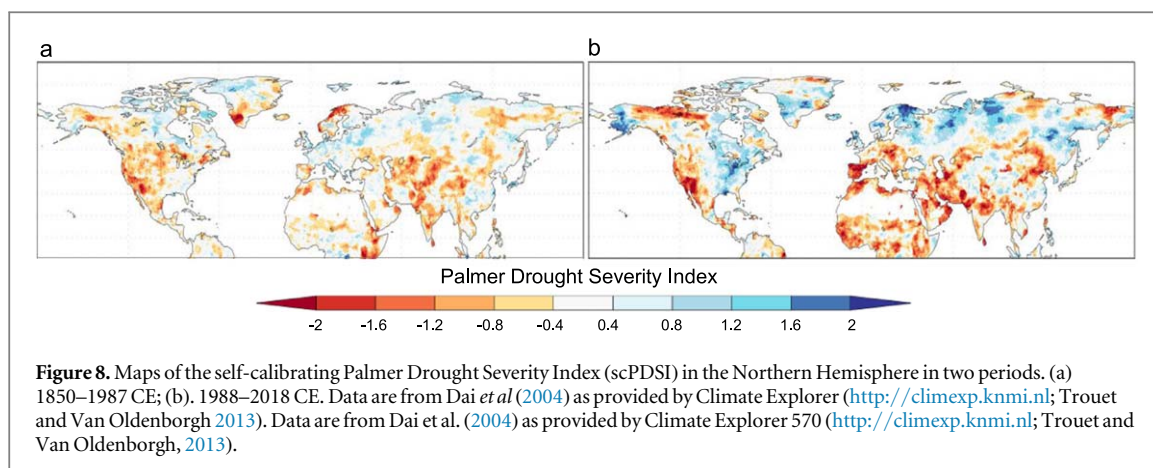
However, the time-series is not stationary, as it shows by two distinct discontinuities (trend breaks) in *c.* 1759 and *c.* 1987 (figure 6(b), red arrows), identified by the Standard Normal Homogeneity Test (SNHT) for the double shift (Alexandersson and Moberg 1997) and Mann-Whitney-Pettitt statistic (Pettitt 1979). The estimated mean ASD is equal to $4.35 \, \text{m}^3 \, \text{s}^{-1}$ ($\pm 0.37 \, \text{m}^3 \, \text{s}^{-1}$ standard deviation) in the initial segment of the time-series (1601–1759 CE) and $4.08 \, \text{m}^3 \, \text{s}^{-1}$ ($\pm 0.39 \, \text{m}^3 \, \text{s}^{-1}$ standard deviation) in the second (1760–1987 CE). A sudden drop can be observed, with $3.60 \, \text{m}^3 \, \text{s}^{-1}$ ($\pm 0.45 \, \text{m}^3 \, \text{s}^{-1}$ standard deviation), in the third period (1988–2020 CE). The change-point shows, however, that it is already from the year 1759 that the ASD starts a decline from which it will never return, which was confirmed by the stastistically significant Mann-Kendall downward trend test ($S = 33764$, $Z = 2370$, $p < 0.01$). This difference was also obtained using Gumbel diagrams (figure 7). For return periods of less than 100 years, the time-frame 1988–2020 CE behaves differently from the previous two. In fact, the interpolating line of the Gumbel diagram in figure 7(c) deviates from that of the previous periods (dashed lines in figures 7(a), (b)), reflecting a markedly different distribution of data in the most recent period.

The last discontinuity (in the year 1987) marks a reduction of about $0.82 \, \text{m}^3 \, \text{s}^{-1}$ respect to the first period 1601–1759, a decline in spring discharge which was only interrupted by the wet years of 2009 and 2010 (Fiorillo and Guadagno 2012). It is notable that the absolute minimum, $2.68 \, \text{m}^3 \, \text{s}^{-1}$, falls in 1761, i.e. before the first change-point. In fact, with six and eight consecutive months of drought, the drought index (*DI*) values for 1760 and 1761 (supplementary table S1, Discharge Reconstruction, column O) reflect the extraordinary and long drought of 1760–1761, which affected harvests and compromised the agronomic and hydrological systems of southern Italy (Ferrari 1977, p. 184, our translation):

> The drought that occurred in the year 1761 was memorable and worthy of note in terms of eternity: a similar one happened in the year 1680. […] from the autumn of the 1760 it did not rain neither in December nor much in the November, January was full of snow but with very little water. In February it rained very little and hardly wet the surface of the Earth; April, May, June and August it never rained, and between so much heat occurred.

Other phases with ASD lower than its mean value coincide with a multi-decadal drought in the first half of the 18th century, and at the turn of the 20th century (figure 6(b)), according to documentary data derived from Diodato and Bellocchi (2011). Figure 6(b) also illustrates the range of dominating climatic conditions that have led to a deficit in spring discharge since about the end of the 20th century (ISPRA 2021). An important consideration is that the depletion in spring discharge after *c.* 1987 reached a mean value with ~10-year return period of $\sim 3.6 \, \text{m s}^{-1}$, which is more than one standard deviation below the mean of the entire time-series. This

Figure 6. Annual spring discharge and climatic patterns over the 1601–2020 CE period in the Caposele aquifer. (a) 21-year moving window (red line) of spring discharge low-extreme (10th percentile); (b) Evolution (red arrows indicating the change-point years of 1759 and 1987) of the annual spring discharge reconstructed over the 1601–1920 CE period, joined to the observed time-series (1921–2020 CE) (light blue line), with over-imposed 11-year Gaussian filter (bold blue line) and long-term mean (horizontal dashed blue line); the left *y*-axis is in log-scale; (c) Wavelet power spectrum with Morlet basis function for reconstructed spring discharge; the bounded colours identify areas of 0.10 significance level; the black bell-shaped contour marks the boundary between the reliable region and the region above the contour where edge effects occur (Hammer *et al* 2001).

Figure 7. Gumbel plots of the annual spring discharge time-series as a function of return period in the Caposele aquifer. (a) 1601–1759 CE (until the 1759 change-point); (b) 1760–1987 CE (transition period between the 1759 and 1987 change-points); (c) 1988–2020 CE (latest and warmest period after the 1987 change-point). The interpolating lines are reported with 95% confidence intervals. The interpolating line of graph (c) overlaps (dashed lines) to graphs (a) and (b).

Figure 8. Maps of the self-calibrating Palmer Drought Severity Index (scPDSI) in the Northern Hemisphere in two periods. (a) 1850–1987 CE; (b). 1988–2018 CE. Data are from Dai *et al* (2004) as provided by Climate Explorer (http://climexp.knmi.nl; Trouet and Van Oldenborgh 2013). Data are from Dai et al. (2004) as provided by Climate Explorer 570 (http://climexp.knmi.nl; Trouet and Van Oldenborgh, 2013).

pattern is easier to interpret if we look at the bold red line in figure 6(a). This line considers the low-end spring discharge (10th percentile), so we can see a slight statistically significant decline in this trend as well (Mann-Kendall test p ∼ 0.00). It can also be observed that the sudden decline falls at the ASD change-points, which reinforces the influence that lower values (10th percentile) have on the critical passages and crossings in the outcome of the spring discharge time-series. This result is important because it suggests a water-deficit scenario that could create a crisis for the aqueduct linked to this source in the coming years—if this downward trend were to continue. This is consistent with the persistent succession of low-rainfall years and drought periods since *c.* 1980, also obtained using different time-series and lower data density (Polemio and Casarano 2008).

The two change-point years we have identified mark different cyclic (solar-ocean) patterns, which further studies could help to explain or clarify for their possible role in underpinning the ASD dynamics in the Mediterranean. In particular, the wavelet power spectrum (figure 6(c)) mainly shows a significant periodicity of ∼60 years in the central part of the LIA, reflecting the periodicity of the Atlantic Multidecadal Oscillation (AMO) (Wang *et al* 2017), i.e. the variability of the sea-surface temperature of the North Atlantic Ocean (Burroughs 2003). However, a significantly longer cycle includes the period from the first change-point (*c.* 1759) to the present, associated with the quasi-secular (∼80–100 years) cycle of solar activity (Gleissberg 1958). During the recent warming period (which includes the second change-point), significant high-frequency periodicities tend rather to mirror the well-known ∼22-year Sunspot cycle (consisting of two ∼11-year cycles with opposite polarities; Schwabe 1843, Hale *et al* 1919).

The estimated values of the Hurst exponent above 0.65 (0.73 and 0.66 with R/S and variance ration methods, respectively) indicate that the reconstructed ASD time-series is linked to long-term memory (which in turn reflects the influences on drought occurrence of large-scale climate systems), implying that there is some dependency structure that favours the predictability of the time-series. The persistence of the decrease in spring discharge at the Caposele station is consistent with the general long-term decrease in river discharge observed over the last five centuries in the Mediterranean region (García-Ruiz *et al* 2011). Also in North America, Lamoureux *et al* (2006) found a decline in spring discharge since the mid-17th century, due to a decrease in snow cover during this period. We can also frame the recent discharge trend detected in this study with changes in spring discharge reflected in soil water content on a global scale (e.g. Dai *et al* 2004), which may mean that the climate change underlying the drought extends over different spatial scales and does not just affect small areas. In fact, figure 8 shows that several areas in the Northern hemisphere have experienced negative values of the Palmer Drought Severity Index (scPDSI, where 'sc' stands for self-calibrating; Wells *et al* 2014) in recent decades (1988–2018 CE; figure 8(a)) compared to 1850–1987 CE (i.e. after the 1987 change-point that we have detected in the Caposele ASD time-series). Not explicitly bounded, the scPDSI typically ranges from –4 (extreme drought) to +4 (extremely wet). The orange and red areas in the legend of figure 8(b) (scPDSI values roughly below –1.2) indicate an emphasis of hydrological droughts across central and southern Europe. The Mediterranean region, in particular, appears to be among the most affected areas with strongly negative scPDSI values, which in turn may have led to a major reduction in spring discharge. The decline of springs in recent times may have been exacerbated by a more general cause, namely man's containment of freshwater and groundwater extraction requiring more water from civil society (Karabil *et al* 2021).

4. Conclusion and outlook

The continuous decline of the spring discharges in the Cervialto Mountains could be largely a response of the groundwater system to climate change (mainly precipitation and temperature) during the last two decades. The

spring discharge at the Caposele station reflects the fact that rainfall-runoff data showed the important impact of climatic variations on the hydrogeological system. It can be concluded that the underground storage zone has an important influence on the outflow of the karst springs, which depends on the precipitation of the previous two or three years. However, other phenomena are also important, such as air temperature, the type of precipitation and the duration of snow cover. Intermittent or continuous drought can also affect spring discharges. However, during drought periods, erratic precipitation and higher temperature are present, and the spring can be strongly affected by these concomitant negative conditions, which are unfavourable for maintaining the same mean spring flow over long periods.

The present findings suggest that research should focus on the capacity of Mediterranean territories to address, respond to and overcome the impacts of climate change on groundwater sources. The spring discharge time-series used is unique in its length (1601–2020 CE), allowing this study to make interpretations about essential elements for medium- to long-term water resource management planning by regional authorities to ensure a sustainable water supply for local communities. However, it is difficult for forecasting systems to consider anthropogenic changes (beyond natural changes) such as over-pumping and to be implemented for predicting water shortages due to human pressures. In particular, it is difficult to understand to which future projection the spring discharge can be attributed to the different modes of climate variability in the Mediterranean region and, likely, whether it can be based on responses to multiple forcing agents. The Mediterranean region is indeed considered a sensitive environment, where wet and dry areas cannot be expected to perform equally well from one year to the next, but adapt their pressure on the environment according to the prevailing climatic situation (Mulligan *et al* 2004). Modern drought conditions—combined with the increased demand for water and human land mismanagement—may contribute to the process of water resource degradation already evident in Mediterranean areas.

Acknowledgments

Data availability statement

All data that support the findings of this study are included within the article (and any supplementary files).

Author contributions

N D and G B developed the original research design and collected and analysed the historical documentary data. N D, F C L, F F, L E and G B wrote the article together and made the interpretations together. All authors reviewed the final manuscript.

Competing interests

The authors declare no competing interests.

ORCID iDs

Fredrik Charpentier Ljungqvist ⓘ https://orcid.org/0000-0003-0220-3947

References

Ait Brahim Y *et al* 2018 Multi-decadal to centennial hydro-climate variability and linkage to solar forcing in the Western Mediterranean during the last 1000 years *Sci. Rep.* **8** 17446

Alexandersson H and Moberg A 1997 Homogenization of Swedish temperature data. Part I: homogeneity test for linear trends *Int. J. Climatol.* **17** 25–34

Anchukaitis K J and Smerdon J E 2022 Progress and uncertainties in global and hemispheric temperature reconstructions of the Common Era *Quat. Sci. Rev.* **286** 107537

Belov I, Kabašinskas A and Sakalauskas L 2006 A study models of stock markets *Inf. Technol. Control.* **35** 34–56

Braconnot P and Vimeux F 2020 Past and future contexts for climate and water-cycle variability, and consequences for the biosphere *Past Global Changes Magazine* **28** 4–5

Burroughs W J 2003 *Weather Cycles* (Cambridge: Cambridge University Press)

Caloiero T, Coscarelli R and Ferrari E 2018 Application of the innovative trend analysis method for the trend analysis of rainfall anomalies in southern Italy *Water Resour. Manage.* **32** 4971–83

Cao R, Jia X, Huang L, Zhu Y, Wu L and Shao M 2018 Deep soil water storage varies with vegetation type and rainfall amount in the Loess Plateau of China *Sci. Rep.* **8** 12346

Chen H, Hu K, Nie Y and Wang K 2017 Analysis of soil water movement inside a footslope and a depression in a karst catchment, Southwest China *Sci. Rep.* **7** 2544

Civita M V and Rostagno K 2014 Le risorse dinamiche della Sorgente Sanità in Caposele (Sud Italia) *Acque Sotterranee-Italian Journal of Groundwater* **31** 9–24 (in Italian)

Coles S 2001 *An Introduction to Statistical Modeling of Extreme Values* (London: Springer)

Costall A R, Harris B D, Teo B, Schaa R, Wagner F M and Pigois J P 2020 Groundwater through flow and seawater intrusion in high quality coastal aquifers *Sci. Rep.* **10** 9866

Cruz M G, Hernandez E A and Uddameri V 2021 Vulnerability assessment of agricultural production systems to drought stresses using robustness measures *Sci. Rep.* **11** 21648

Cui J *et al* 2020 Vegetation forcing modulates global land monsoon and water resources in a CO_2-enriched climate *Nat. Commun.* **11** 5184

Cuthbert M O *et al* 2019 Observed controls on resilience of groundwater to climate variability in sub-Saharan Africa *Nature* **572** 230–4

Dai A, Trenberth K E and Qian T 2004 A global data set of Palmer Drought Severity Index for 1870–2002: relationship with soil moisture and effects of surface warming *J. Hydrometeorol.* **5** 1117–30

Dawid P and Senn S 2011 Statistical model selection *Simplicity, Complexity and Modelling* ed M Christie *et al* (Hoboken NJ: Wiley) pp 11–33

De Lorenzo G 1939 Geologia e geografia fisica di Leonardo da Vinci *Annali dei Lavori Pubblici* **77** 233–53 [in Italian]

De Vita P, Allocca V, Manna F and Fabbrocino S 2012 Coupled decadal variability of the North Atlantic Oscillation, regional rainfall and karst spring discharges in the Campania region (southern Italy) *Hydrol. Earth Syst. Sci.* **16** 1389–99

Diodato N *et al* 2017 Historical evolution of slope instability in the Calore River Basin, Southern Italy *Geomorphology* **282** 74–84

Diodato N and Bellocchi G 2008 Drought stress patterns in Italy using agro-climatic indicators *Clim. Res.* **36** 53–63

Diodato N and Bellocchi G 2011 Historical perspective of drought response in Mediterranean Italy *Clim. Res.* **49** 189–200

Diodato N, Bellocchi G, Fiorillo F and Ventafridda G 2017 Case study for investigating groundwater and the future of mountain spring discharges in Southern Italy *J. Mt. Sci.* **14** 1791–800

Diodato N and Fiorillo F 2013 Complexity-reduced in the hydroclimatological modelling of aquifer's discharge *Water and Environ. J.* **27** 170–6

Diodato N, Ljungqvist C F and Bellocchi G 2019 A millennium-long reconstruction of damaging hydrological events across Italy *Sci. Rep.* **9** 9963

Diodato N, Ljungqvist C F and Bellocchi G 2021 Climate patterns in the world's longest history of storm-erosivity: the Arno River Basin, Italy *Front. Earth Sci.* **9** 637973

Diodato N and Mariani L 2007 Testing a climate erosive forcing model in the Po River Basin *Clim. Res.* **33** 195–205

Dorber M, Arvesen A, Gernaat D and Verones F 2020 Controlling biodiversity impacts of future global hydropower reservoirs by strategic site selection *Sci. Rep.* **10** 21777

Dubois E, Doummar J, Pistre S and Larocque M 2020 Calibration of a lumped karst system model and application to the Qachqouch karst spring (Lebanon) under climate change conditions *Hydrol. Earth Syst. Sci.* **24** 4275–90

Ducci D and Tranfaglia G 2008 *Effects of climate change on groundwater resources in Campania (southern Italy)* (London, Special Publications: Geological Society) 288, pp 25–38

Esit M, Kumar S, Pandey A, Lawrence D M, Rangwala I and Yeager S 2021 Seasonal to multi-year soil moisture drought forecasting *npj Clim. Atmos. Sci.* **4** 16

Esposito E, Pece R, Porfido S and Tranfaglia G 2001 Hydrological anomalies connected to Earthquakes in southern Apennines (Italy) *Nat. Hazards Earth Syst. Sci.* **1** 137–44

Ferrari U 1977 *Giovan Battista Moio, Gregorio Susanna: Diario di quanto Successe in Catanzaro dal 1710 al 1769* (Chiaravalle: Effe Emme) [in Italian]

Fiorillo F 2009 Spring hydrographs as indicators of droughts in a karst environment *J. Hydrol.* **373** 290–301

Fiorillo F and Doglioni A 2010 The relation between karst spring discharge and rainfall by the cross-correlation analysis *Hydrogeol. J.* **18** 1881–95

Fiorillo F and Guadagno F M 2010 Karst spring discharges analysis in relation to drought periods, using the SPI *Water Resour. Manage.* **2** 1867–84

Fiorillo F and Guadagno F M 2012 Long karst spring discharge time series and droughts occurrence in Southern Italy *Environ. Earth. Sci.* **65** 2273–83

Fiorillo F, Pagnozzi M and Ventafridda G 2015 A model to simulate recharge processes of karst massifs *Hydrol. Process.* **29** 2301–14

Fuccello A 2021 Dante e la meteorologia *Rivista di Meteorologia Aeronautica* **75** 6–17 [in Italian]

García-Ruiz J M, López-Moreno J I, Vicente-Serrano S M, Lasanta–Martínez T and Beguería S 2011 Mediterranean water resources in a global change scenario *Earth-Sci. Rev.* **105** 121–39

Gates J B, Edmunds W M, Ma J and Sheppard P R 2008 A 700-year history of groundwater recharge in the drylands of NW China *Holocene* **7** 1045–54

Gleissberg W 1958 The eighty-year Sunspot cycle *J. Br. Astr. Assoc.* **68** 1148–52

Hale G E, Ellerman F, Nicholson S B and Joy A H 1919 The magnetic polarity of Sun-spots *Astrophys. J.* **49** 153–78

Hammer Ø, Harper D A T and Ryan P D 2001 Past: paleontological statistics software package for education and data analysis *Palaeontol. Electron.* **4** 9

Hare D K, Helton A M, Johnson Z C, Lane J W and Briggs M A 2021 Continental-scale analysis of shallow and deep groundwater contributions to streams *Nat. Commun.* **12** 1450

Hsu K-C, Yeh H F, Chen Y-C, Lee C-H, Wang C-H and Chiu F-C 2012 Basin-scale groundwater response to precipitation variation and anthropogenic pumping in Chih-Ben watershed, Taiwan *Hydrogeol. J.* **20** 499–517

Hurst H E 1951 Long-term storage capacity of reservoirs *Trans. Am. Soc. Civil Eng.* **116** 770–808

ISPRA 2021 *Gli indicatori del clima in Italia nel 2020—Anno XVI* (Rome: Istituto Superiore per la Protezione e la Ricerca Ambientale) [in Italian]

Jaafarzadeh M S, Tahmasebipour N, Haghizadeh A, Pourghasemi R H and Rouhani H 2021 Groundwater recharge potential zonation using an ensemble of machine learning and bivariate statistical models *Sci. Rep.* **11** 5587

Karabil S, Sutanudjaja E H, Lambert E, Bierkens M F P and Van de Wal R S W 2021 Contribution of land water storage change to regional sea-level rise over the twenty-first century *Front. Earth Sci.* **9** 627648

Kogan F, Guo W and Yang W 2020 Near 40-year drought trend during 1981–2019 Earth warming and food security *Geomatics, Nat. Hazards Risk* **11** 469–90

Lamoureux S F, Stewart K A, Forbes A C and Fortin D 2006 Multidecadal variations and decline in spring discharge in the Canadian middle Arctic since 1550 AD *Geophys. Res. Lett.* **33** L02403

Leone G, Pagnozzi M, Catani V, Ventafridda G, Esposito L and Fiorillo F 2021 A hundred years of Caposele spring discharge measurements: trends and statistics for understanding water resource availability under climate change *Stoch. Environ. Res. Risk Assess.* **35** 345–70

Li B, Rodell M, Sheffield J, Wood E and Sutanudjaja E 2019 Long-term, non-anthropogenic groundwater storage changes simulated by three global-scale hydrological models *Sci. Rep.* **9** 10746

Liang W and Zhang M 2021 Summer and winter precipitation in East Asia scale with global warming at different rates *Commun. Earth Environ.* **2** 150

Lim K J, Engel B A, Tang Z, Muthukrishnan S, Choi J and Kim K 2006 Effects of calibration on L-THIA GIS runoff and pollutant estimation *J. Environ. Manage.* **78** 35–43

Ljungqvist F C *et al* 2019 Summer temperature and drought co-variability across Europe since 850 CE *Environ. Res. Lett.* **14** 084015

Ljungqvist F C, Krusic P J, Brattström G and Sundqvist H S 2012 Northern Hemisphere temperature patterns in the last 12 centuries *Clim. Past* **8** 227–49

Ljungqvist F C, Krusic P J, Sundqvist H S, Zorita E, Brattström G and Frank D 2016 Northern Hemisphere hydroclimatic variability over the past twelve centuries *Nature* **532** 94–8

Mankin J S, Seager R, Smerdon J E, Cook B I and Williams A P 2019 Mid-latitude freshwater availability reduced by projected vegetation responses to climate change *Nat. Geosci.* **12** 983–8

Manna F, Walton K M, Cherry J A and Parker B L 2019 Five-century record of climate and groundwater recharge variability in southern California *Sci. Rep.* **9** 18215

Matthews J A and Briffa K R 2005 The 'Little ice age': Re-evaluation of an evolving concept *Geogr. Ann.* **87** 17–36

Miller G H *et al* 2012 Abrupt onset of the Little Ice Age triggered by volcanism and sustained by sea-ice/ocean feedbacks *Geophys. Res. Lett.* **39** L02708

Mulligan M, Burke S M and Concepcion M 2004 Climate change, land-use change and the 'desertification' of Mediterranean Europe *Recent Dynamics of the Mediterranean Vegetation and Landscape* ed S Mazzoleni *et al* (Chichester: Wiley) pp 259–79

Nash J E and Sutcliffe J V 1970 River flow forecasting through conceptual models part I - a discussion of principles *J. Hydrol.* **10** 282–90

Nolin A F, Tardif J C, Conciatori F, Kames S, Meko D M and Bergeron Y 2021 Multi-century tree-ring anatomical evidence reveals increasing frequency and magnitude of spring discharge and floods in eastern boreal Canada *Glob Planet Change* **199** 103444

Nowreen S *et al* 2020 Groundwater recharge processes in an Asian mega-delta: hydrometric evidence from Bangladesh *Hydrogeol. J.* **28** 2917–32

Ouyang Y, Zhang J, Feng G, Wan Y and Leininger T D 2020 A century of precipitation trends in forest lands of the lower mississippi river alluvial valley *Sci. Rep.* **10** 12802

Pauling A, Luterbacher J, Casty C and Wanner H 2006 Five hundred years of gridded high-resolution precipitation reconstructions over Europe and the connection to large-scale circulation *Clim. Dyn.* **26** 387–405

Pettitt A N 1979 A non-parametric approach to the change-point problem *Appl. Stat.* **28** 126–35

Pfister C and Wanner H 2021 *Climate and society in Europe: The last Thousand Years* (Bern: Haupt Verlag)

Philipps F M, Walvoord M A and Small E E 2004 Effects of environmental change on groundwater recharge in the Desert Southwest *Groundwater Recharge in a Desert Environment: the Southwestern United States* ed J F Hogan *et al* (Washington DC: American Geophysical Union) pp 273–94

Pokhrel Y *et al* 2021 Global terrestrial water storage and drought severity under climate change *Nat. Clim. Chang.* **11** 226–33

Polemio M and Casarano D 2008 Climate change, drought and groundwater availability in southern Italy *Climate Change and Groundwater* ed W Dragoni and B S Sukhija (London: Geological Society) pp 39–51

Qiu J, Zipper S C, Motew M, Booth E G, Kucharik C J and Loheide S P 2019 Nonlinear groundwater influence on biophysical indicators of ecosystem services *Nat. Sustain.* **2** 475–83

Ramírez-Pacheco J C R, Torres-Roman D, Total-Cruz H and Vargas L E 2008 High-performance tool for the test of long-memory and self-similarity *Simulation Technologies in Networking and Communications* ed A-S K Pathan *et al* pp 93–113

Ranjan P and Pankaj K P 2021 Spring protection: step towards water security and sustainable rural water supply *Annals of the Romanian Society for Cell Biology* **25** 1216–22

Rao M P *et al* 2020 Seven centuries of reconstructed Brahmaputra River discharge demonstrate underestimated high discharge and flood hazard frequency *Nat. Commun.* **11** 6017

Saccò M *et al* 2021 Rainfall as a trigger of ecological cascade effects in an Australian groundwater ecosystem *Sci. Rep.* **11** 3694

Schwabe S H 1843 Sonnenbeobachtungen im Jahre 1843 *Astron. Nachr.* **21** 233–6 [in German]

SIMN *Hydrological Annals* (Rome, Italy: Servizio Idrografico e Mareografico Nazionale) 1921–97 [in Italian]

Smirnov N 1948 Table for estimating the goodness of fit of empirical distributions *Ann. Math. Stat.* **19** 279–81

Sperna Weiland F C, van Beek L P H, Kwadijk J C J and Bierkens M F P 2011 Global patterns of change in discharge regimes for 2100 *Hydrol. Earth Syst. Sci. Discuss.* **8** 10973–1014

Stepanek P 2007 *AnClim—Software for Time Series Analysis (for Windows)* (Brno, Czech Republic: Department of Geography, Faculty of Natural Sciences, Masaryk University)

Tegel W *et al* 2020 Higher groundwater levels in western Europe characterize warm periods in the Common Era *Sci. Rep.* **10** 16284

Toreti A *et al* 2011 A note on the use of the standard normal homogeneity test (SNHT) to detect inhomogeneities in climatic time series *Int. J. Climatol.* **31** 630–2

Trouet V and Van Oldenborgh G J 2013 KNMI Climate Explorer: a web-based research tool for high-resolution paleoclimatology *Tree Ring Res.* **69** 3–13

Wang J *et al* 2017 Internal and external forcing of multidecadal Atlantic climate variability over the past 1,200 years *Nat. Geosci.* **10** 512–7

Wang J *et al* 2018 Recent global decline in endorheic basin water storages *Nat. Geosci.* **11** 926–32

Wanner H, Pfister C and Neukom R 2022 The variable European Little Ice Age *Quaternary Sci. Rev.* **287** 107531

Wells N, Goddard S and Hayes M J 2014 A self-calibrating Palmer Drought Severity Index *J. Climate* **17** 2335–51

Willmott C J, Rowe C M and Mintz Y 1985 Climatology of the terrestrial seasonal water cycle *J. Climatol.* **5** 589–606

Wu W Y *et al* 2020 Divergent effects of climate change on future groundwater availability in key mid-latitude aquifers *Nat. Commun.* **11** 3710

Xu S *et al* 2021 Investigating groundwater-lake interactions in the Laurentian Great Lakes with a fully-integrated surface water-groundwater model *J. Hydrol.* **594** 125911

Zhang J, Liu K and Wang M 2020 Seasonal and interannual variations in China's groundwater based on GRACE data and multisource hydrological models *Remote Sens.* **12** 845